Desalination and Water Treatment
www.deswater.com
doi: 10.5004/dwt.2023.29588

294 (2023) 89–99
May

Separation of organic pesticide (insecticide): lambda-cyhalothrin from wastewater using magnetic carbon nanocomposites

Muhammad Zahoor[a,*], Azmat Ullah[b], Jawad Ikram[b], Muhammad Naveed Umar[c], Riaz Ullah[d]

[a]*Department of Biochemistry, University of Malakand, Chakdara Dir Lower, 18800. Khyber Pakhtunkhwa, Pakistan, email: mohammadzahoorus@yahoo.com (M. Zahoor)*
[b]*Department of Chemistry, Govt. Degree College Mingora, Swat, Khyber Pakhtunkhwa, Pakistan, emails: azmatullah9499@gmail.com (A. Ullah), jisameer1414@gmail.com (J. Ikram)*
[c]*Department of Chemistry, University of Liverpool, UK, email: m.naveed-umar@liverpool.ac.uk (M.N. Umar)*
[d]*Department of Pharmacognosy, College of Pharmacy, King Saud University, Riyadh 11451, Saudi Arabia, email: rullah@ksu.edu.sa (R. Ullah)*

Received 19 December 2022; Accepted 25 April 2023

ABSTRACT

In this study, a potato wastes based magnetic carbon nanocomposite (PMCNC) was synthesized and explored for its possible applications as adsorbent in removal of lambda-cyhalothrin from synthetically contaminated water. The nanocomposites were characterized through energy-dispersive X-ray, X-ray diffraction analysis, scanning electron microscopy, Fourier-transform infrared spectrophotometry, zero-point charge (pH_{pzc}) and thermogravimetric/differential thermal analysis. For the demonstration of adsorption efficiency of the nanocomposite, batch adsorption experiments were carried out. Maximum removal of selected pollutant was achieved in 30 min. Several kinetic and isotherm models were applied to the sorption kinetics and isothermal data. The pseudo-second-order kinetics fitted well the data. The X_{max} (maximum adsorption) at 50°C was recorded as 14.025 mg/g with K_2 (pseudo-second-order kinetics constant) value of 0.0162 and R^2 value of 0.99. The adsorption isotherm data fitted well the Langmuir isotherm model. The optimum pH for the removal of lambda-cyhalothrin was achieved at pH 5. 0.1 g of PMCNC was used as optimum dose in all experiments. The negative value of Gibbs free energy reveals that the removal of lambda-cyhalothrin is a spontaneous process. Due to the excellent adsorption capability and easy separation from slurry after use through the application of magnet the PMCNC can be effectively used as an effective sorbent alternative to activated carbon for the removal of inorganic and organic contaminants from aquatic media. This nanocomposite could compete with other adsorbents in the field of surface chemistry warranting further experimentation.

Keywords: Pesticide; Insecticide; Lambda-cyhalothrin; Magnetic carbon nanocomposites; Batch adsorption

1. Introduction

Pesticides keeps plants safe against pests and diseases, however, their use on large scale can lead to a number of health complications both human and plants. Pesticides being bio-accumulative in tissue can harm non-targeted creatures, particularly marine animals [1]. Intoxication of pesticides badly effect human health with symptoms like severe headache, reproductive disorders, cancer and imbalance of endocrine hormones. Pesticides are considered as a primary

* Corresponding author.

pollutant of aquatic environment due to its high solubility in water [2]. According to a UN report on contaminants, each day, approximately twenty lac tons of industrial and agricultural effluents are discharged into water reservoirs that badly effecting the water quality as well lives of flora and fauna living there [3–5].

Pesticides being synthetic compounds are mostly non-biodegradable whereas in other cases have long half-lives if degradable and accumulates in various environmental compartments. Organic pesticides are extensively utilized to cope agricultural pests throughout the world. The commonly used organic pesticides (insecticides) are lambda-cyhalothrin (L-C), cypermethrin, and dimethoate etc. They are very stable, having high half-lives [6] with no specificity of their mode of action. Due to excessive usage of organic pesticide or their residues have been identified in certain foods, drinks, dairy products, water reservoirs, fruits, and in animal feedstuff [7–9].

L-C (Fig. 1) is an organic insecticide that is extensively utilized to regulate a number of pests in a wide range of crops. It is also utilized for the control of the harmful flying insects. They are directly sprayed in water ponds and in residential areas to regulate pests [10,11]. L-C is predominantly poisonous to aquatic organisms [12]. L-C disturb the neural system of aquatic organisms ultimately paralyzing or even leading to death. The residual concentration of L-C in food due to its massive uses in field is reported to be less than 0.2 mg/kg [13].

The pyrethrin has been enumerated in water from agricultural watersheds in concentration range of 0.11 to 0.14 mg/L, and in sediments in concentration range of 0.00314 mg/L to 0.315 mg/g of dry weight [14,15].

Being utilized in high amounts their removal from aquatic environment has been attempted by employing both classical and modern methods. Among these methods adsorption has produced far reaching results. Among the adsorbents reported so far activated carbon due to its small size and consequently large surface area has been found to be a versatile adsorbent [16–19]. However, like every material object it is also associated with a number of drawbacks like long settling times due to which one have to wait for days to separate it after use from slurry. Iron oxide, being magnetic and heavy particles if used as adsorbent can easily be removed from water through the application of magnet and even under gravity they settled down. However, iron oxide has very little surface area which render its use as adsorbent [20].

To get better separation of activated carbon after use from slurry, scientist have deposited iron oxide on its surface in small amount to successfully introduce magnetic character in it which then was easily removed from slurry through the application of magnet [20,21]. The little decrease in surface area of activated carbon due to deposition of iron oxide is compensated with easy separation through the application of magnet. Such composites have been explored in very limited studies and with very few biomass sources. Potato peel is a waste by-product and to convert it into a valuable product, in this study an attempt was made to convert it into magnetic carbon nano composite [22]. The prepared composite was characterized by various instrumental techniques whereas batch adsorption experiments were performed to estimate its adsorption capacity, kinetics constants and thermodynamics parameters for the adsorption of L-C).

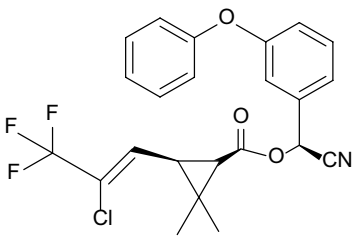

Fig. 1. Structure of lambda-cyhalothrin.

2. Experimental set-up

2.1. Reagents and material

The biomass precursors of potato peels were collected from local chips shop in Swat District of KP (Pakistan). The insecticide lambda-cyhalothrin was collected in pure form from Shafi Agricultural Company, Mingora Swat. All the chemicals and materials utilized in the current research work were of analytical grade (purity ≈ 100%). Double distilled water (deionized water in mass titration method) was used in all experimental work.

2.2. Preparation of potato peel based magnetic carbon nanocomposites

Potato peel biomass precursors were collected from a local chips shop in Swat, KP (Pakistan). The waste biomass of potato peels was washed frequently with boiled water. The sample was then dried for one week in the shade. 0.05 mol/L ferric chloride hexahydrate and 0.025 mol/L ferrous sulfate heptahydrate solutions were prepared in 200 mL distilled water is separate beaker. Both solutions were then mixed in a 1,000 mL beaker. After this, the dried sample of potato peels was added to the mixture of ferric chloride and ferrous sulfate. After mixing the slurry was agitated vigorously at 343 K for 5–10 min. After that, a 5 mol/L concentrated solution of NaOH was introduced dropwise to the mixture to adjust till pH 10. After 1 h stirring the mixture was cooled. After cooling the mixture was filtered. The solid residue was then charred in a specially designed container for 60–90 min at 250°C under nitrogen atmosphere. After cooling the charred product was neutralized through 0.2 mol/L HCl solution. After neutralization the end product was washed several times with distilled water to achieve the neutral pH. At last, the product was oven dried for 10–12 h at 343 K. The dried sample was then stored in a sealed glass reagent bottle [20–22].

2.3. Characterization of the composites

Energy-dispersive X-ray (EDX: Inca 200 Oxford Instruments, UK) was used to determine the elemental composition of potato wastes based magnetic carbon nanocomposite (PMCNC) whereas the surface morphology was visualized by scanning electron microscopy (SEM) at 20 kV accelerating voltage. X-ray diffraction (XRD) analysis was used to determine the iron cubic structures in the composite utilizing mono-chromatic Cu K_{α} rays having wavelength of

1.5418 Å. The X-ray originator was set at 30 mA current and 40 kV at 10 min^{-1} speed with 2θ/θ as the scan rate and range, respectively. The Fourier-transform infrared (FTIR) spectrum of PMCNC was recorded with Shimadzu 8201PC Fourier-Transform Infrared Spectrophotometer (Japan), employing KBr pellet method. Thermogravimetric and differential thermal analysis (TG/DTA) under N_2 atmosphere was performed using a diamond series TG/DTA PerkinElmer (USA), US analyzer with Al_2O_3 as a reference source. Nanocomposites were subjected to temperatures ranging from 50°C to 600°C. Point of zero charge (pH_{pzc}) of the composite was determined using mass titration method.

2.4. Adsorption studies

In kinetic studies glass reagent bottles having a specific quantity of PMCNC were added to 25 mL of known concentration of L-C. The slurry was then shaken at 150 rpm for different intervals of time. Different kinetic models were applied to the adsorption kinetics data.

In isotherm studies different concentration of L-C were taken in glass reagent bottles containing a known amount of PMCNC. The slurry was shaken for 1 h time. Different isotherm models like Langmuir and Freundlich were employed to the adsorption isotherm data to estimate the isothermal constants. The effect of pH on adsorption was evaluated from 2 to 12 pH. For optimum dose of PMCNC the sorbent dosage was varied from 0.01 to 0.3 g. van't Hoff equation was employed for the determination of various thermodynamic parameters. In each experiment the solution was filtered using Wattman filter paper. The residual concentration of L-C was determined after sorption experiment using a double beam UV/visible spectrophotometer at 580 nm. The following equations were used to evaluate the residual concentration of L-C in solution.

$$X_q = \left(S_i - S_e\right)\frac{V}{m} \tag{1}$$

$$\%\ \text{Removal} = \frac{\left(S_i - S_e\right)}{S_i} \times 100 \tag{2}$$

where S_i and S_e represents the initial and equilibration concentrations of L-C (mg/L), X_q represents the amount of L-C adsorbed on the surface of PMCNC (mg/g), V represents volume of L-C in liters (L), and m represents the quantity of PMCNC with in grams (g).

3. Results and discussion

3.1. Characterization of the magnetic carbon nanocomposite

The biomass wastes of potato peels were used to prepare magnetic carbon nanocomposites. To check the magnetic behavior of the prepared nanocomposite a magnetic bar was conveyed near the composite. The composite was completely stick to the bar magnet, confirm the magnetic characteristic of the composite.

3.1.1. EDX analysis of PMCNC

Fig. 2 displays the elemental composition of PMCNC. Lower percentage of carbon content was attributed due to impregnation of Fe_3O_4 microporous texture of the carbonaceous matter. Other elements found in PMCNC were oxygen, chlorine and nitrogen. Small percentages of S, Si, Na, P and Ca were also present in PMCNC.

3.1.2. SEM images of PMCNC

Fig. 3 shows the SEM images of PMCNC with high and low magnification. The figure gives a clear photograph of PMCNC. The composite has various shapes and particle size. White patches in SEM images represent the water of crystallization of Fe_3O_4 and presence of moisture. The black spots represent the carbon content of PMCNC. The SEM images also shows the porous texture of PMCNC. The mean diameter of PMCNC calculated from SEM images varies from 50 to 70 nm.

The mushy nature of porous surfaces indicates a homogeneous dispersion of Fe_3O_4 nanoparticles in carbonaceous matter. The crystalline structure of Fe_3O_4 is likewise slightly cubic in character.

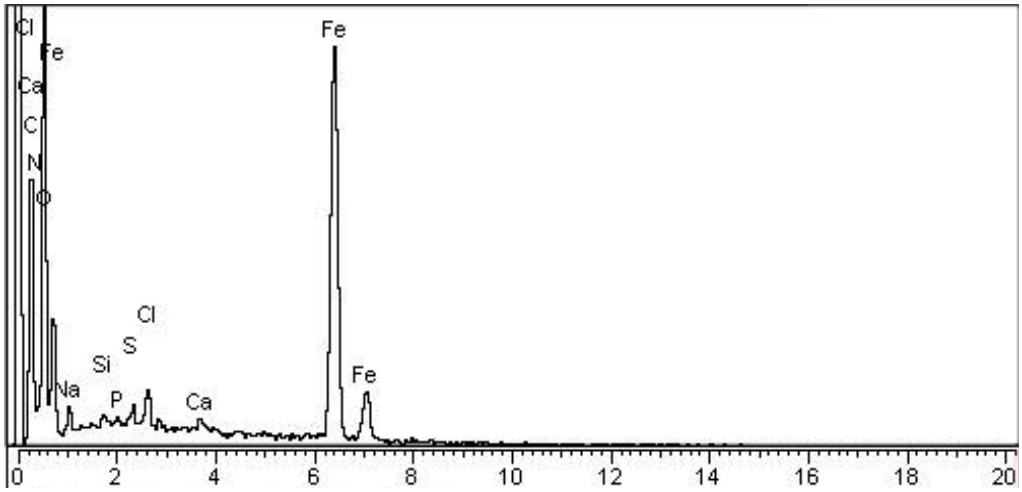

Fig. 2. Energy-dispersive X-ray analysis of PMCNC.

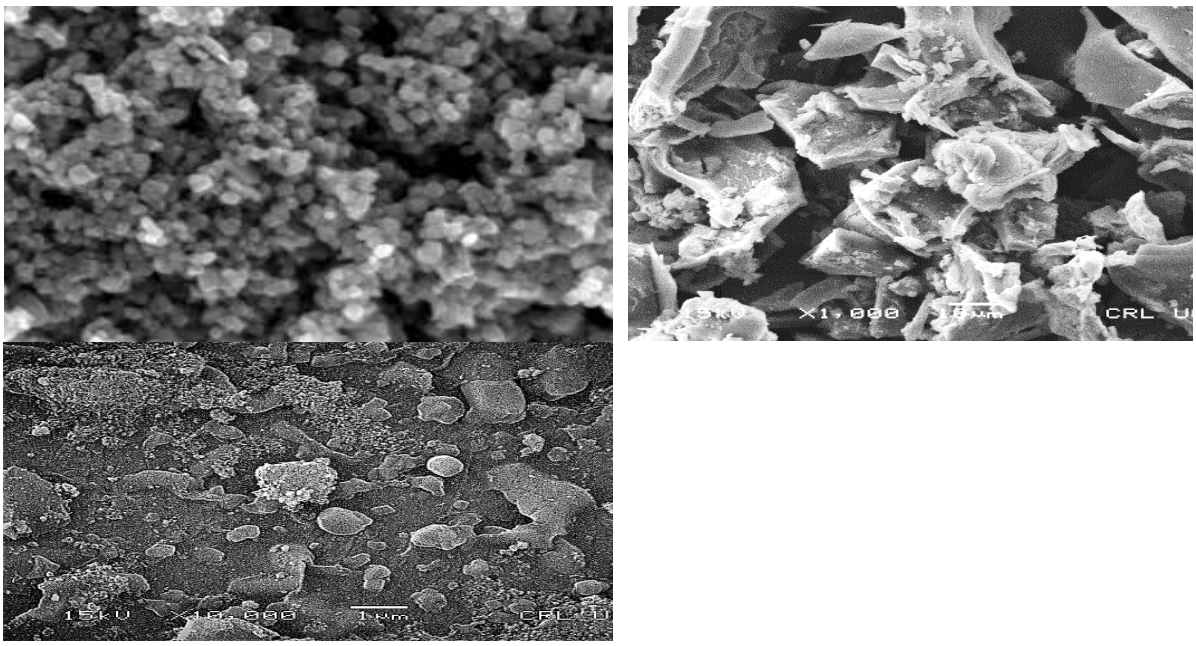

Fig. 3. Scanning electron microscopy images of PMCNC.

3.1.3. XRD analysis of PMCNC

XRD arrays of PMCNC is shown in Fig. 4. It is a well-known and valuable analytical technique used for the determination of crystallinity of a substance. The XRD diffractogram patterns of PMCNC composite at 2θ° value of 31°, 36.7°, 45°, 54°, 58.95°, and 63.5°, corresponding to indices 220, 331, 400, 442, 531 and 532 indices, respectively. All these diffraction peaks show the characteristic peaks of magnetite and maghemite. All these indices at 2θ° represent the cubic crystalline structure Fe_3O_4 in PMCNC.

3.1.4. Fourier-transform infrared analysis

The FTIR spectra of PMCNC composite is given in Fig. 5. The FTIR spectra of PMCNC display different peaks with broad bands in the range of 3,480 and 3,210 cm^{-1}. It is due to stretching vibrations of phenolic and carboxylic –OH group. These peaks correspond to physically adsorbed water on the surface of PMCNC. The two narrow peaks at 3,000–2,800 cm^{-1} range corresponds to C–H alkanes. Various peaks in the region of 1,450–1,600 cm^{-1} corresponds to C=C aromatic. The Peaks in the region of 1,300–1,000 cm^{-1} corresponds to alcoholic and ethereal functional groups. The peak in the region of 575–580 cm^{-1} corresponds to magnetite iron oxide.

3.1.5. Thermogravimetric/differential thermal analysis of PMCNC

Fig. 6. represents the TG/DTA pictogram of PMCNC. The TGA pictogram of PMCNC elucidate that the composite is thermally quite stable and shows resistance to loss in mass at high temperature. In the early stage in the temperature range of 40°C to 100°C a 6%–10% loss in mass occurs due to dehydration. Around 250°C another loss in mass occurs due to dehydration of physically adsorbed water in the texture of PMCNC. Up to a temperature of 550°C, PMCNC experienced uninterrupted weight loss. Because FeO is thermodynamically stable. At 570°C the decrease in mass occurs due to burning of carbon and phase change of FeO. Above this temperature PMCNC shows no additional mass depression. The end product is a char and ash combination.

The DTA pictogram of PMCNC shows three endothermic peaks in the range of 30°C–490°C.

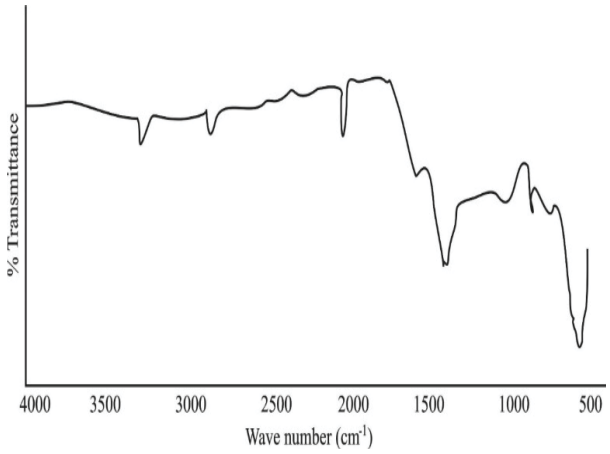

Fig. 4. X-ray diffractogram patterns of PMCNC.

3.1.6. Zero-point charge (pH_{pzc}) of PMCNC

Fig. 7 elucidates the pH_{pzc} of PMCNC. For this purpose, pH_{pzc} of PMCNC was determined through mass titration method. Different quantities of PMCNC was added to fresh distilled water and resulting pH values were measured after

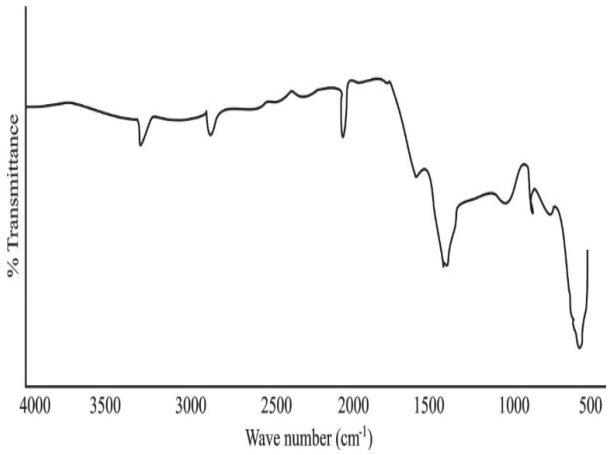

Fig. 5. Fourier-transform infrared spectroscopy analysis plot of PMCNC.

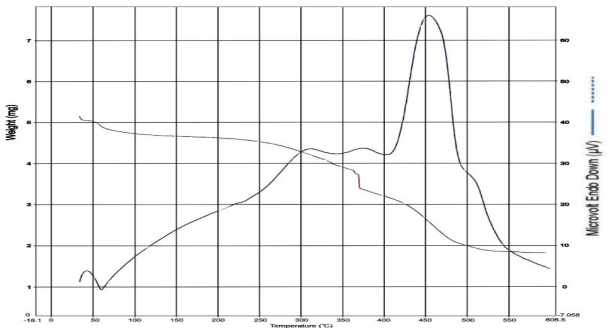

Fig. 6. Thermogravimetric/differential thermal analysis plot of PMCNC.

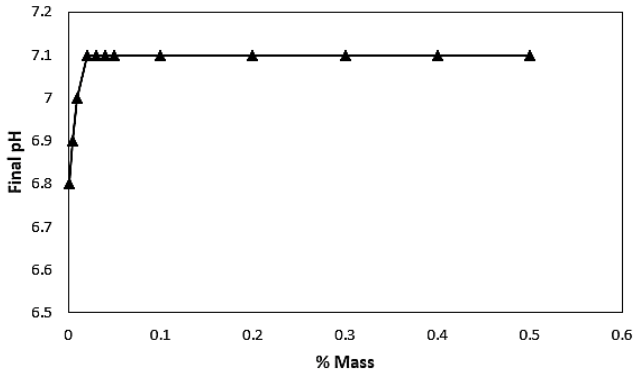

Fig. 7. Mass titration plot of PMCNC for pH_{pzc}.

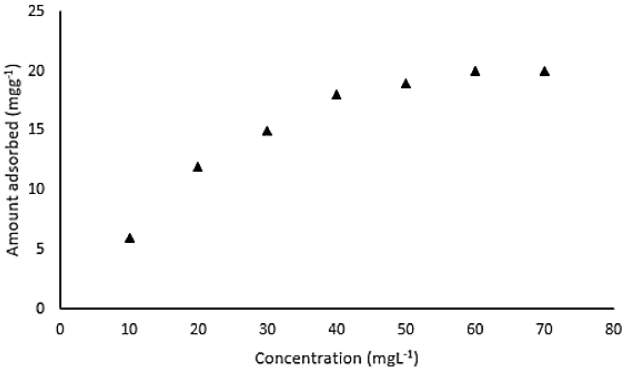

Fig. 8. Adsorption isotherm plot of lambda-cyhalothrin onto PMCNC.

24 h of equilibration. Typical values of PMCNC/distilled water by weight were 0.001%, 0.005%, 0.01%, 0.02%, 0.03%, 0.04%, 0.05%, 0.1%, 0.2%, 0.3%, 0.4% and 0.5% were used under the atmospheric environment of nitrogen gas. The reagent bottles of PMCNC/distilled water were wrapped. They are placed on a shaker. The mixtures in reagent bottles were for 24 h. The pH_{pzc} of PMCNC was found to be 7.1. This value is were nearer to those reported for magnetic activated carbon by Mohan et al. 6.80 [23], Mao et al. 7.30 [24], Tu et al. 7.64 [25], Zhang et al. 8.1 [26], and Ullah et al. [20–22].

3.2. Adsorption isotherm studies of L-C

The adsorption of L-C on the surface of PMCNC were studied using Giles isotherm [27]. The Giles isotherm of the L-C is shown in Fig. 8. The adsorption isotherm of L-C on the surface of PMCNC is C type, which was formerly described by Mao et al. [28], Nazari et al. [29], and Rivera-Utrilla et al. [30].

The impact of initial concentration of L-C on its sorption onto PMCNC from aquatic media was studied at 298 K. During isotherm studies 0.1 g of PMCNC was added to various concentrations of sorbate. The slurry was stirred for 1 h. During adsorption isotherm studies the initial concentration of L-C was varied from 10 to 70 mg/L. It was observed that the extent of adsorption was increased with the rise in concentration of the L-C and attained constant values at higher concentrations Fig. 8. The constant value of sorption at higher concentration may be due to the saturation of available active sites on the surface of PMCNC.

For quantitative determination of the sorption of L-C onto PMCNC, various isotherm models such as Langmuir and Freundlich models were used.

The linear form of the Langmuir isotherm is given by the following equation:

$$\frac{S_e}{X_q} = \frac{1}{K_L X_m} + \frac{S_e}{X_q} \tag{3}$$

where X_q is the extent of L-C adsorbed in mg/g, S_e is the equilibrium concentration of the L-C in mg/L, X_m in mg/g is the maximum sorption capacity of PMCNC and K_L in L/mg is Langmuir constant (energy of sorption). The Langmuir plot of L-C adsorption was obtained by plotting (S_e/X_q) against equilibrium concentration (S_e) for PMCNC. The Langmuir plot is shown in Fig. 9. The Langmuir constants X_m and K_L were calculated from the slope and intercept of the linear plot. The values are tabulated in Table 1. The lower sorption capability of PMCNC is due to the obstruction of micro pores impregnation of carbonaceous material due to iron oxide.

The Freundlich isotherm is an empirical equation employed to explain heterogeneous systems. The linear form of the Freundlich isotherm model is given as.

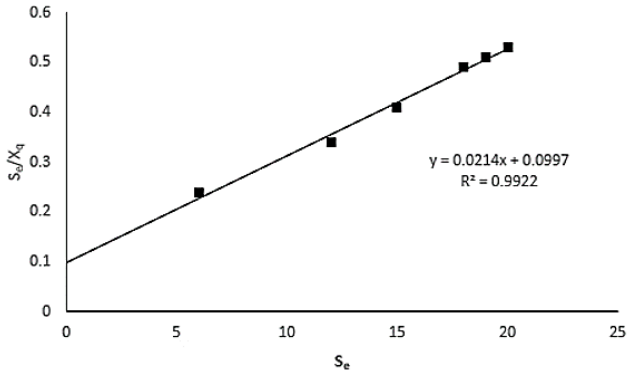

Fig. 9. Langmuir plot of lambda-cyhalothrin onto PMCNC.

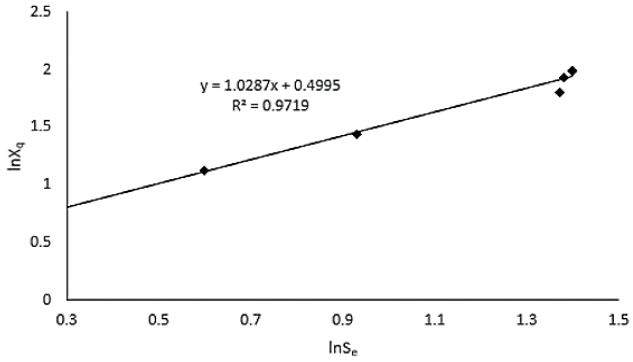

Fig. 10. Freundlich plot of lambda-cyhalothrin onto PMCNC.

$$\ln X_q = \ln k + \ln \frac{S_e}{n} \tag{4}$$

where S_e is the equilibrium concentration in mg/L of L-C, X_q is the extent of L-C adsorbed in mg/g on the surface of PMCNC, while k and n are Freundlich constants. k and n are related to the sorption capacity and sorption intensity, respectively.

The Freundlich plot is achieved by plotting $\ln S_e$ vs. $\ln X_q$. The Freundlich plot is shown in Fig. 10. Various isotherm parameters of Freundlich model like k and $1/n$ are calculated from the slope and intercept of the linear plot. The values of Freundlich constants and R^2 are listed in Table 1.

3.3. Adsorption kinetics of lambda-cyhalothrin

In adsorption kinetics study, 50 mg/L of L-C was added to reagent bottles containing 0.1 g of PMCNC. The mixture was stirred for different intervals of time using different temperature.

The adsorption kinetics plot of L-C at various temperatures is presented in Fig. 11. From the plot it is evident that the rate of adsorption is high in the initial 25–30 min. The higher rate of adsorption in the initial 30 min is due to the availability of active surface sites on PMCNC. As time increases the rate of adsorption of L-C on the surface of PMCNC decreases. The lower rate of adsorption with the passage of time is due to saturation of surface-active sites

Table 1
Isotherm parameters for the adsorption of lambda-cyhalothrin onto PMCNC

Langmuir isotherm		Freundlich isotherm	
X_m (mg/g)	21.00	K (mg/g)	87
K_L (L/mg)	0.03	$1/n$	0.97
R^2	0.992	R^2	0.972

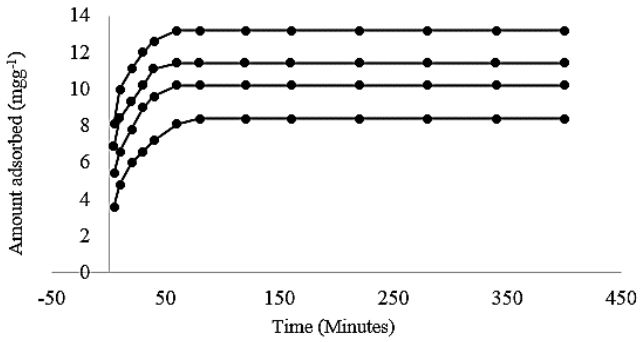

Fig. 11. Sorption kinetics and equilibration plot of lambda-cyhalothrin onto PMCNC.

on PMCNC. A time is reached after 1 h the line become horizontal with x-axis. It shows the complete saturation of active sites on PMCNC with L-C molecules. So, 1 h time was selected as equilibration time for all experimental studies for the decontamination of L-C on PMCNC. Various kinetic models were applied to the sorption kinetics data of L-C to know the mechanism of sorption.

3.3.1. Pseudo-first-order kinetics

To examine the sorption kinetics data of L-C adsorption on PMCNC, the Lagergren pseudo-first-order kinetic equation was employed.

$$\log\left(S_i - S_e\right) = \log\left(X_{\max}\right) - K_1 t \tag{5}$$

where $X_{\max}$ represents the magnitude of L-C sorption at time t in mg/g, S_i represents the initial concentration of L-C, while S_e represents the equilibration concentration of L-C in mg/L, and K_1 represents the pseudo-first-order rate constant in min^{-1}.

A linear plot of pseudo-first-order kinetic model is obtained by plotting time (on x-axis) and $\ln(X_{qe}-X_{qt})$ on y-axis. The pseudo-first-order kinetic model is presented in Fig. 12. The value of K_1 and $X_{\max}$ is obtained from the slope and intercepts of the straight line. The smaller value of R^2 shows that the reaction of L-C adsorption on the surface of PMCNC does not follow first order kinetics. Similarly, the calculated value $X_{\max}$ of L-C on the surface of PMCNC deviate from experimental value. Different values of kinetic parameters of pseudo-first-order kinetic model are tabulated in Table 2.

3.3.2. Pseudo-second-order kinetics model

The pseudo-second-order reaction can be practiced to describe the stepwise explanation of a reaction kinetics.

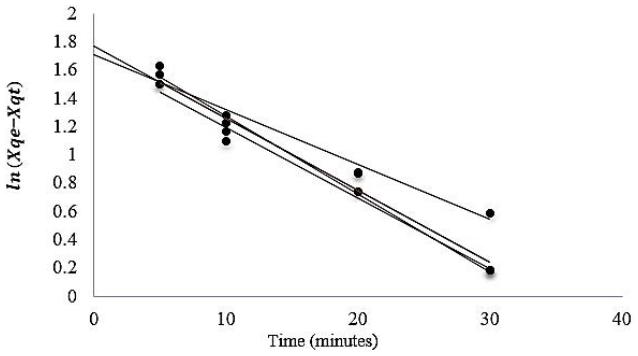

Fig. 12. Pseudo-first-order kinetics adsorption plot of lambda-cyhalothrin on PMCNC.

Table 2
Pseudo-first-order kinetic parameters of lambda-cyhalothrin onto PMCNC

Parameters	293 K	303 K	313 K	323 K
X_{max}	0.791	0.990	0.980	0.920
K_1	1.700	1.800	1.820	1.700
R^2	0.96	0.98	0.98	0.98

The linear form of pseudo-second-order kinetics is given in Eq. (6).

$$\frac{t}{X_{qt}} = \frac{1}{K_2 X_{max}^2} + \frac{1}{X_{max}} \times t \quad (6)$$

where X_{qt} and X_{max} of the L-C in mg/g sorbed onto the surface of PMCNC at time t and equilibrium time in minutes, respectively. K_2 is the pseudo-second-order soroption rate constant (g/mg·min).

The linear lot of above-mentioned model is obtained by plotting t/X_{qt} on y-axis and time in minutes on x-axis. Different values of X_{max} and K_2 were designed from the slope and intercept of the linear plot. Various kinetic parameters of pseudo-second-order kinetic model obtained from linear plot are tabulated in Table 3. From Fig. 13 it is clearer that pseudo-second-order kinetics model fitted better to the adsorption kinetics data of L-C onto PMCNC. Since the value of R^2 is nearer to unity. Apart from the value of R^2 the calculated maximum adsorption (X_{max}) of L-C have an approximately equal value to the experimentally determined value of L-C. It can be concluded that pseudo-second-order reaction kinetic fully explains the sorption of L-C on PMCNC. From the resultant data we can concluded that the sorption of L-C on magnetic PMCNC is favoured by the presence of the carbon active sites.

3.3.3. Intraparticle diffusion model

The adsorption kinetic data of L-C was also verified for Weber's intraparticle diffusion model. This model exlain the sorption of sorbate molecules onto the surface of sorbent through phenomenon of diffusion. The linear form of intraparticle diffusion model is given in Eq. (7).

Table 3
Pseudo-second-order kinetic parameters of lambda-cyhalothrin onto PMCNC

Parameters	293 K	303 K	313 K	323 K
X_{max}	9.120	11.300	12.300	14.000
K_2	0.0120	0.0130	0.0170	–
R^2	0.994	0.997	0.996	0.999

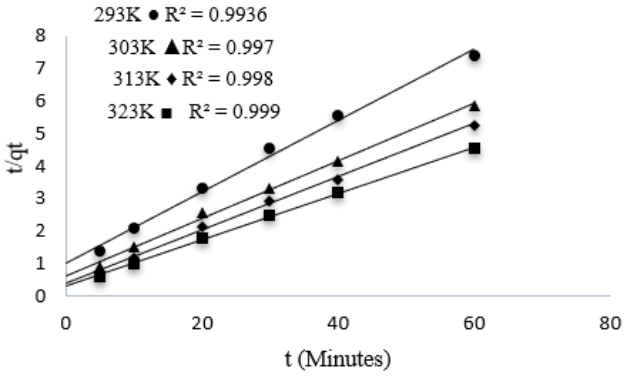

Fig. 13. Pseudo-second-order kinetic of lambda-cyhalothrin onto PMCNC.

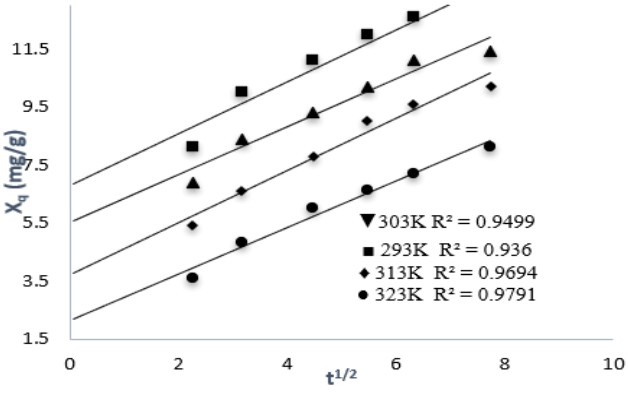

Fig. 14. Plot of intraparticle diffusion model of lambda-cyhalothrin onto PMCNC.

$$X_{qt} = K_3 t^{1/2} + C \quad (7)$$

where X_{qt} in mg/g is the extent of L-C molecules sorbed at t time, K_3 is adsorption rate constant of intraparticle diffusion model (mg/g·min$^{-0.5}$) and C (mg/g) is the thickness of the boundary layer. The graph (Fig. 14) of intraparticle diffusion model was achieved by plotting X_{qt} vs. $t^{1/2}$ for the removal of L-C onto PMCNC. Various kinetic parameters of intraparticle diffusion model is obtained from the slope and intercept of linear plot. If the linear part of the curves passes through the origin of the plot, it can be concluded that intraparticle diffusion is not the only rate-controlling process. The plot of intraparticle diffusion model show an initial curve followed by linear relationship of the plot. The

initial curve of the plot can be explained by the boundary layer effect while the linearity of plot corresponds to the intraparticle diffusion phenomena [31,32]. The linear portion of the plot don't pass through plot origin shows that intraparticle diffusion phenomenon is not the only controlling step for the removal of L-C onto PMCNC. Various parameters of intraparticle diffusion model are tabulated in Table 4.

3.3.4. Mechanism of lambda-cyhalothrin adsorption on the surface of potato-based nanocomposite

Fig. 15 Illustrates the mechanism of L-C onto the surface of PMCNC. Removal of L-C onto the surface of PMCNC from aqueous solution through adsorption process is due to electrostatic forces of attraction, π–π interaction, hydrogen bonding and the formation of complex [33].

- pH of the surrounding solution played an important role in the removal of pesticides through electrostatic forces of attraction mechanism. At pH less than 7 ($pH < pH_{pzc}$), the surface of nanocomposite gained a positive charge due to protonation of –OH group. As a result, OH_2^+ formation took place. The produced positively charged nanocomposite then interact with the oppositely charged L-C.
- The FTIR spectra of nanocomposite confirms the presence of H-bonding. The presence of free –OH group on the surface of nanocomposite may act as H-acceptor and the strongly electronegative N and O of L-C as hydrogen donor forming hydrogen bonds.
- L-C form complex with Fe of nanocomposite through N and O atoms of L-C.

Table 4
Intraparticle diffusion kinetic model of lambda-cyhalothrin onto PMCNC

Parameters	293 K	303 K	313 K	323 K
C	6.700	5.520	3.700	2.140
K_3	0.900	0.823	0.970	–
R^2	0.936	0.9499	0.9694	0.9791

3.4. Effect of pH

The L-C sorption on the surface of PMCNC was studied as a function of pH. The pH values was varied from 2–12. The results are specified in Fig. 16. The results show that as pH increases from 2–5, the sorption capacity of PMCNC increases gradually. It is due to protonation of N and O

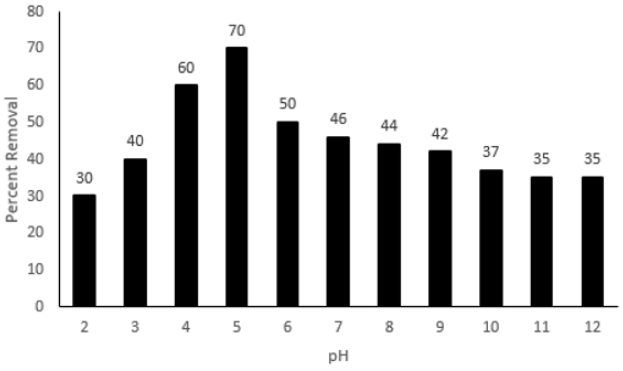

Fig. 16. pH plot for the removal of lambda-cyhalothrin onto PMCNC.

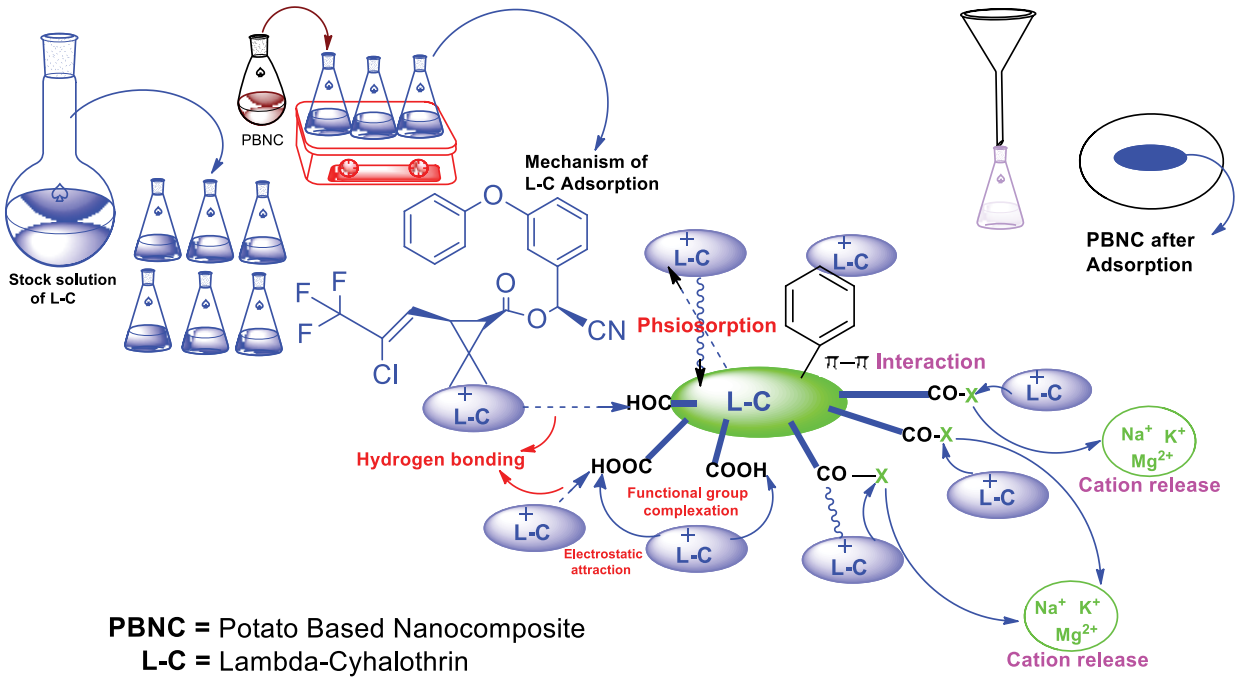

Fig. 15. Mechanism of lambda-cyhalothrin adsorption on the surface of potato-based nanocomposite.

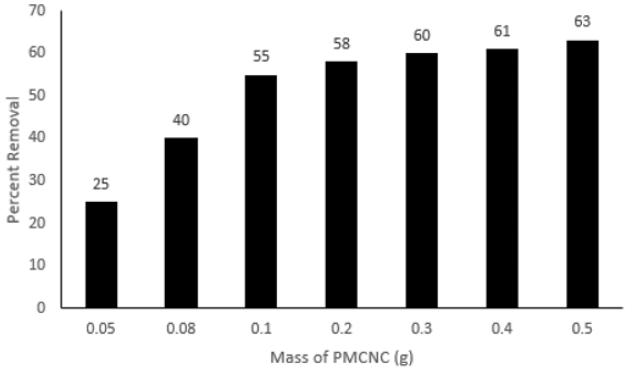

Fig. 17. Adsorbent dosage plot for the removal of lambda-cyhalothrin onto PMCNC.

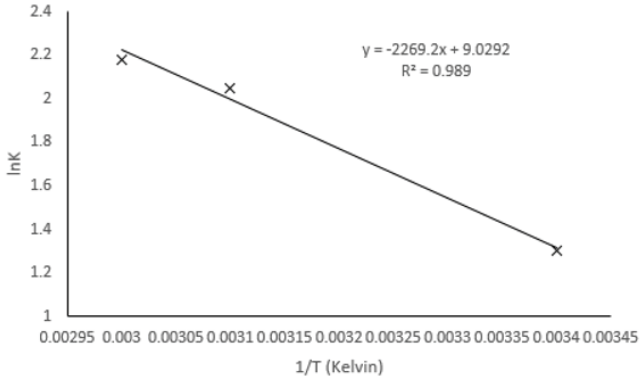

Fig. 18. van't Hoff plot for the removal of lambda-cyhalothrin onto PMCNC.

containing functional groups. Above pH 5, the adsorption capacity of PMCNC decreases rapidly. It is largely because the pH value of the solution affects the surface charges of the PMCNC. At acidic pH, the surface of PMCNC has a positive charge due to the protonation phenomenon. As pH rises from acidic to neutral and then to alkaline, the surface of PMCNC becomes negatively charged due to the deprotonation reaction.

3.5. Effect of adsorption dosage

The impact of sorbent dosage was varied from 0.05–0.5 g at initial L-C concentration of 20 mg/L was determined at 298 K and pH 5. The results in Fig. 17 show that the L-C removal increases quickly with rise in sorbent dose, that is, from 0.05 to 0.1 g and onwards rise is slow. It may be due to increase in number of adsorption sites. So, 0.1 g of the PMCNC dose was selected and used in various experiments.

3.6. Adsorption thermodynamics parameters

For the determination of adsorption thermodynamics, the adsorption experiment was carried out at 293, 313, and 333 K. The van't Hoff calculation was utilized to define the standard enthalpy ($\Delta H°$) and standard entropy ($\Delta S°$) of the sorption method.

$$\ln K = \frac{\Delta S°}{R} - \frac{\Delta H°}{RT} \tag{8}$$

where K is a constant known as sorption co-efficient distribution (L/g), $\Delta H°$ is enthalpy, $\Delta S°$ is entropy, T is temperature in Kelvin and R is a general gas constant.

The van't Hoff graphs (Fig. 18) was obtained by plotting ln$K$ against 1/T. Different values of K is calculated from the ratio of L-C adsorbed and equilibrium concentration at different temperatures. The values of $\Delta H°$ and $\Delta S°$ is obtained from the slope and intercept of linear plot, respectively.

Standard free energy ($\Delta G°$) were calculated at different temperature using the following equation.

$$\Delta G° = \Delta H° - T\Delta S° \tag{9}$$

Table 5
Thermodynamic parameters of lambda-cyhalothrin onto PMCNC

Thermodynamic parameters	Temperature (K)		
	293	313	333
Standard enthalpy ($\Delta H°$)	–34 kJ/mol	–	–
Standard entropy ($\Delta S°$)	94 kJ/mol	–	–
Standard Gibbs free energy ($\Delta G°$)	–13.3 kJ/mol	–19.3 kJ/mol	–23.7 kJ/mol

Table 6
Maximum adsorption capacities of some nanocomposites

Lung et al. [34]	14.925 and 20.492 mg/g
Wang et al. [35]	20 μg
Motaghi et al. [36]	25.2 mg/g
Duman et al. [37]	5.3 and 16.3 mg/L
Choumane and Benguella [38]	7.49 mg/g
This work	14.025 mg/g

where the calculated values of $\Delta G°$ are –13.3, –19.3 and –23.7 kJ/mol at 293, 313, and 333K, respectively (Table 5). The negative values of $\Delta G°$ at various temperatures specify the spontaneous nature of the process. It also shows high affinity of L-C molecules for PMCNC. The rise in $\Delta G°$ with the rise in temperature displays that the route of L-C sorption is more promising at high temperature.

3.7. Comparison with other nanocomposites

Table 6 shows the adsorption capabilities of various nanocomposites for the decontamination of pesticides from aquatic media [34–38]. From all these results it is evident that PMCNC made from biomass precursors of potato have quite agreeable sorption capacity and can easily be detached from solution using external magnet.

4. Conclusion

In this study, potato-based magnetic carbon nanocomposite (PMCNC) was prepared from waste biomass precursors of Potato peels. The novel sorbent was tried for the decontamination of lambda-cyhalothrin (an insecticide) from aquatic media. Different sorption isotherm and kinetics models were employed to explain the sorption experimental information. The sorption kinetics results fit to pseudo-second-order kinetics model, while sorption isotherm results fitted well to Langmuir isotherm model than Freundlich isotherm model. The values of standard entropy ($\Delta S°$) and standard enthalpy ($\Delta H°$) were positive, while that of Gibbs free energy ($\Delta G°$) was negative. At higher temperature (333 K) the value of $\Delta G°$ was high as compared with that at 293 and 313 K, confirms that the process of adsorption is favorable at high temperature. Maximum adsorption occurs at acidic pH. The optimum dosage employed in all experiment was 0.1 g. From the adsorption data it is concluded that PMCNC can be used as efficient sorbent for the decontamination of was and can compete with other sorbents in the field of surface chemistry.

Author statement

All authors have checked and approved the final version of manuscript.

Acknowledgement

The authors extend their appreciation to the researchers supporting Project Number (RSP2023R110) King Saud University, Riyadh, Saudi Arabia, for financial support.

References

[1] J. Campo, A. Masiá, C. Blasco, Y. Picó, Occurrence and removal efficiency of pesticides in sewage treatment plants of four Mediterranean River Basins, J. Hazard. Mater., 263 (2013) 146–157.
[2] I.C. Yadav, N.L. Devi, J.H. Syed, Z. Cheng, J. Li, G. Zhang, K.C. Jones, Current status of persistent organic pesticides residues in air, water, and soil, and their possible effect on neighboring countries: a comprehensive review of India, Sci. Total Environ., 511 (2015) 123–137.
[3] V. Babu, M. Selvanayagam, E.I. Cengiz, E. Unlu, Histopathology of lambda-cyhalothrin on tissues (gill, kidney, liver and intestine) of *Cirrhinus mrigala*, Environ. Toxicol. Pharmacol., 24 (2007) 286–291.
[4] N. Rambabu, K. Jamil, Evaluation of cytogenetic effects of lambda-cyhalothrin on human lymphocytes, J. Biochem. Mol. Toxicol., 19 (2005) 304–310.
[5] Q. Wu, G. Zhao, C. Feng, C. Wang, Z. Wang, Preparation of a graphene-based magnetic nanocomposite for the extraction of carbamate pesticides from environmental water samples, J. Chromatogr. A, 1218 (2011) 7936–7942.
[6] W.A. El-Said, D.M. Fouad, M.H. Ali, M.A. El-Gahami, Green synthesis of magnetic mesoporous silica nanocomposite and its adsorptive performance against organochlorine pesticides, Int. J. Environ. Sci. Technol., 15 (2018) 1731–1744.
[7] C. Gong, J. Lin, J. Lu, X. Zhao, Z. Cai, J. Fu, Advanced treatment of pesticide-containing wastewater using Fenton reagent enhanced by microwave electrodeless ultraviolet, BioMed Res. Int., 2015 (2015) 205903, doi: 10.1155/2015/205903.
[8] C. De Smedt, P. Spanoghe, S. Biswas, K. Leus, P. Van Der Voort, Comparison of different solid adsorbents for the removal of mobile pesticides from aqueous solutions, Adsorption, 21 (2015) 243–254.
[9] N. Tarannum, R. Khan, Cost-Effective Green Materials for the Removal of Pesticides from Aqueous Medium, M. Naushad, E. Lichtfouse, Eds., Green Materials for Wastewater Treatment. Environmental Chemistry for a Sustainable World, Vol. 38, Springer, Cham, 2020. https://doi.org/10.1007/978-3-030-17724-9_5
[10] A.M. Youssef, M.E. El-Naggar, F.M. Malhat, H.M. El Sharkawi, Efficient removal of pesticides and heavy metals from wastewater and the antimicrobial activity of *f*-MWCNTs/PVA nanocomposite film, J. Cleaner Prod., 206 (2019) 315–325.
[11] H. Xia, Removal of Lambda-Cyhalothrin by Water Hyacinth (*Eichornia crassipes*), 2nd International Conference on Bioinformatics and Biomedical Engineering, IEEE, Shanghai, China, 2008, pp. 3446–3450.
[12] C. De Smedt, F. Ferrer, K. Leus, P. Spanoghe, Removal of pesticides from aqueous solutions by adsorption on zeolites as solid adsorbents, Adsorpt. Sci. Technol., 33 (2015) 457–485.
[13] A. Mojiri, J.L. Zhou, B. Robinson, A. Ohashi, N. Ozaki, T. Kindaichi, H. Farraji, M. Vakili, Pesticides in aquatic environments and their removal by adsorption methods, Chemosphere, 253 (2020) 126646, doi: 10.1016/j.chemosphere.2020.126646.
[14] I.A. Saleh, N. Zouari, M.A. Al-Ghouti, Removal of pesticides from water and wastewater: chemical, physical and biological treatment approaches, Environ. Technol. Innovation, 19 (2020) 101026, doi: 10.1016/j.eti.2020.101026.
[15] S. Heydari, L. Zare, H. Ghiassi, Plackett–Burman experimental design for the removal of diazinon pesticide from aqueous system by magnetic bentonite nanocomposites, J. Appl. Res. Water Wastewater, 6 (2019) 45–50.
[16] P.K. Boruah, B. Sharma, N. Hussain, M.R. Das, Magnetically recoverable Fe_3O_4/graphene nanocomposite towards efficient removal of triazine pesticides from aqueous solution: investigation of the adsorption phenomenon and specific ion effect, Chemosphere, 168 (2017) 1058–1067.
[17] W.-W. Tang, G.-M. Zeng, J.-L. Gong, Y. Liu, X.-Y. Wang, Y.-Y. Liu, Z.-F. Liu, L. Chen, X.-R. Zhang, D.-Z. Tu, Simultaneous adsorption of atrazine and Cu(II) from wastewater by magnetic multi-walled carbon nanotube, Chem. Eng. J., 211 (2012) 470–478.
[18] K. Shrivas, A. Ghosale, N. Nirmalkar, A. Srivastava, S.K. Singh, S.S. Shinde, Removal of endrin and dieldrin isomeric pesticides through stereoselective adsorption behavior on the graphene oxide-magnetic nanoparticles, Environ. Sci. Pollut. Res., 24 (2017) 24980–24988.
[19] B. Ouassyla, R. Marouf, O. Fatima, S. Jacques, Sewage sludge adsorbents used to remove lambda cyhalothrin from aqueous phase, Res. J. Chem. Environ., 23 (2019) 53–61.
[20] A. Ullah, M. Zahoor, S. Alam, Removal of ciprofloxacin from water through magnetic nanocomposite/membrane hybrid processes, Desal. Water Treat., 137 (2019) 260–272.
[21] M. Zahoor, A. Ullah, S. Alam, Removal of enrofloxacin from water through magnetic nanocomposites prepared from pineapple waste biomass, Surf. Eng. Appl. Electrochem., 55 (2019) 536–547.
[22] A. Ullah, M. Zahoor, S. Alam, R. Ullah, A.S. Alqahtani, H.M. Mahmood, Separation of levofloxacin from industry effluents using novel magnetic nanocomposite and membranes hybrid processes, BioMed Res. Int., 2019 (2019) 5276841, doi: 10.1155/2019/5276841.
[23] D. Mohan, A. Sarswat, V.K. Singh, M. Alexandre-Franco, C.U. Pittman Jr., Development of magnetic activated carbon from almond shells for trinitrophenol removal from water, Chem. Eng. J., 172 (2011) 1111–1125.
[24] H. Mao, S. Wang, J.-Y. Lin, Z. Wang, J. Ren, Modification of a magnetic carbon composite for ciprofloxacin adsorption, J. Environ. Sci., 49 (2016) 179–188.
[25] Y. Tu, Z. Peng, P. Xu, H. Lin, X. Wu, L. Yang, J. Huang, Characterization and application of magnetic biochars from corn stalk by pyrolysis and hydrothermal treatment, BioResources, 12 (2017) 1077–1089.
[26] S. Zhang, H. Chen, L. Tao, C. Huang, M. Jiang, Z. Zhou, Magnetic activated carbon for efficient removal of Pb(II) from aqueous solution, Environ. Eng. Sci., 35 (2018) 111–120.

[27] C.H. Giles, T.H. MacEwan, S.N. Nakhwa, D. Smith, 786. Studies in adsorption. Part XI. A system of classification of solution adsorption isotherms, and its use in diagnosis of adsorption mechanisms and in measurement of specific surface areas of solids, J. Chem. Soc., 786 (1960) 3973–3993.
[28] H. Mao, S. Wang, J.-Y. Lin, Z. Wang, J. Ren, Modification of a magnetic carbon composite for ciprofloxacin adsorption, J. Environ. Sci., 49 (2016) 179–188.
[29] G. Nazari, H. Abolghasemi, M. Esmaieli, Batch adsorption of cephalexin antibiotic from aqueous solution by walnut shell-based activated carbon, J. Taiwan Inst. Chem. Eng., 58 (2016) 357–365.
[30] J. Rivera-Utrilla, G. Prados-Joya, M. Sánchez-Polo, M.A. Ferro-García, I. Bautista-Toledo, Removal of nitroimidazole antibiotics from aqueous solution by adsorption/bioadsorption on activated carbon, J. Hazard. Mater., 170 (2009) 298–305.
[31] J.N. Genc, E.C. Dogan, Adsorption kinetics of the antibiotic ciprofloxacin on bentonite, activated carbon, zeolite, and pumice, Desal. Water Treat., 53 (2015) 785–793.
[32] W. Plazinski, W. Rudzinski, A. Plazinska, Theoretical models of sorption kinetics including a surface reaction mechanism: a review, Adv. Colloid Interface Sci., 152 (2009) 2–13.
[33] M. El-Kammah, E. Elkhatib, S. Gouveia, C. Cameselle, E. Aboukila, Enhanced removal of thiamethoxam from wastewater using waste-derived nanoparticles: adsorption performance and mechanisms, Environ. Technol. Innovation, 28 (2022) 102713, doi: 10.1016/j.eti.2022.102713.
[34] I. Lung, M.-L. Soran, A. Stegarescu, O. Opriş, Devrinol and triadimefon removal from aqueous solutions using CNT-COOH/MnO_2/Fe_3O_4 nanocomposite, J. Iran. Chem. Soc., 19 (2022) 2031–2039.
[35] W. Zhaokun, J. Zhang, B. Hu, J. Yu, J. Wang, X. Guo, Graphene/Fe_3O_4 nanocomposite for effective removal of ten triazole fungicides from water solution: tebuconazole as an example for investigation of the adsorption mechanism by experimental and molecular docking study, J. Taiwan Inst. Chem. Eng., 95 (2019) 635–642.
[36] H. Motaghi, P. Arabkhani, M. Parvinnia, A. Asfaram, Simultaneous adsorption of cobalt ions, azo dye, and imidacloprid pesticide on the magnetic chitosan/activated carbon@UiO-66 bio-nanocomposite: optimization, mechanisms, regeneration, and application, Sep. Purif. Technol., 284 (2022) 120258, doi: 10.1016/j.seppur.2021.120258.
[37] O. Duman, C. Özcan, T.G. Polat, S. Tunç, Carbon nanotube-based magnetic and non-magnetic adsorbents for the high-efficiency removal of diquat dibromide herbicide from water: OMWCNT, OMWCNT-Fe_3O_4 and OMWCNT-κ-carrageenan-Fe_3O_4 nanocomposites, Environ. Pollut., 244 (2019) 723–732.
[38] F.Z. Choumane, B. Benguella, Removal of acetamiprid from aqueous solutions with low-cost sorbents, Desal. Water Treat., 57 (2016) 419–430.